

Forget Less by Learning Together through Concept Consolidation

Arjun Ramesh Kaushik Naresh Kumar Devulapally Vishnu Suresh Lokhande
 Nalini Ratha Venu Govindaraju
 University at Buffalo, SUNY

{kaushik3, devulapa, vishnulo, nratha, govind}@buffalo.edu

Abstract

Custom Diffusion Models (CDMs) have gained significant attention due to their remarkable ability to personalize generative processes. However, existing CDMs suffer from catastrophic forgetting when continuously learning new concepts. Most prior works attempt to mitigate this issue under the sequential learning setting with a fixed order of concept inflow and neglect inter-concept interactions. In this paper, we propose a novel framework - Forget Less by Learning Together (FL2T) - that enables concurrent and order-agnostic concept learning while addressing catastrophic forgetting. Specifically, we introduce a set-invariant inter-concept learning module where proxies guide feature selection across concepts, facilitating improved knowledge retention and transfer. By leveraging inter-concept guidance, our approach preserves old concepts while efficiently incorporating new ones. Extensive experiments, across three datasets, demonstrates that our method significantly improves concept retention and mitigates catastrophic forgetting, highlighting the effectiveness of inter-concept catalytic behavior in incremental concept learning of ten tasks with at least 2% gain on average CLIP Image Alignment scores.

1. Introduction

Advancements in training, architectures, and datasets have enhanced text-conditioned generative models, enabling photorealistic text-to-image synthesis [3, 31, 34]. Conditional diffusion models facilitate high-fidelity image generation from text prompts and support user control over scene layout and sketches [6, 24, 29, 43]. This level of quality in text-conditioned generative models opens up new avenues for customization and personalization, allowing for the generation of images featuring specific objects or individuals in novel contexts or backgrounds. The ability to precisely capture concepts from reference images and seamlessly integrate them with text prompts is a significant advancement. Early approaches to model customization typically involved

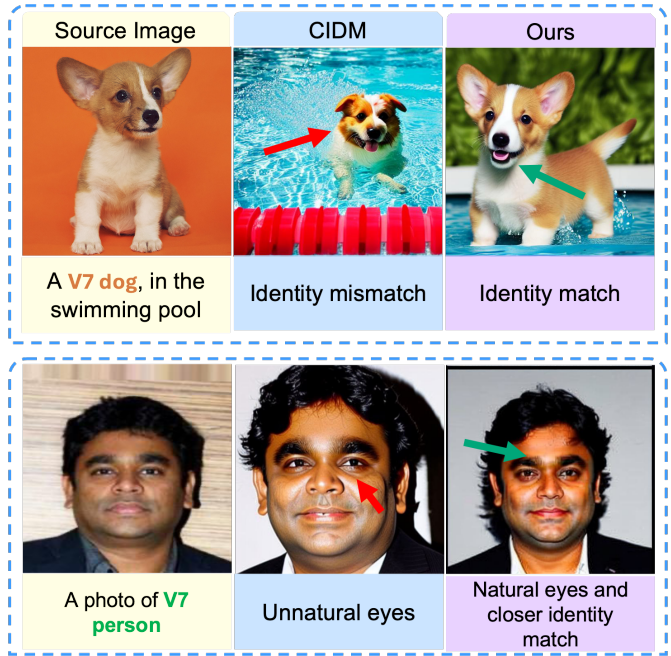


Figure 1. **Forget Less by Learning Together (FL2T)**. Our method focuses on learning G concepts in an order-agnostic incremental learning problem setting with fewer parameters and fewer reference images while also mitigating catastrophic forgetting. Unlike previous works, we leverage inter-concept interactions positively. The above image showcases examples of generated images, with a source image and an associated text prompt (left column) as input. We evaluate the generated image (right column) against the SOTA model CIDM [5] (middle column). The red and green arrows indicate regions of undesirable and desirable qualities, and their reasons are stated below each image.

fine-tuning a subset of model parameters [50] or text token embeddings [7] using a small set of user-provided reference images, often with additional regularization techniques [44]. However, this fine-tuning process, which is required for each new concept, is both time-intensive and computationally costly. As a result, recent efforts have shifted toward developing tuning-free methods that elimi-

nate the need for per-object optimization during inference, thus offering a more efficient and scalable solution for customization.

Concurrently, efforts are underway to expand the capability of model customization beyond a single, individual concept, aiming to seamlessly compose multiple new concepts together. However, this approach introduces additional challenges, such as the integration of unseen concepts and the potential for catastrophic forgetting of previously learned personalized concepts when new concepts are learned in succession through a concept-incremental framework. Additionally, issues like concept neglect may arise when performing multi-concept composition based on user-defined conditions [5, 9]. A common setup in this area involves continuous customization with new, fine-grained concepts that have not been encountered before, typically with only a few examples provided for each new concept. This setup aligns with the concept of continual learning, which focuses on training a model across a sequence of tasks, each with a distinct data distribution, while striving to retain previously acquired knowledge without interference or forgetting.

The continual learning framework provides a promising direction for multi-concept personalization [5, 20, 39]. Fundamentally, multi-concept personalization is closely related to training with larger datasets, as it inherently involves access to a greater number of reference images compared to single-concept personalization [5, 12, 36]. Existing approaches predominantly adopt a sequential concept learning paradigm, where new concepts are learned one after another. While this is practical, it raises the question: *If reference images for all concepts are available from the outset, why not leverage them for simultaneous joint learning?* This paper aims to address this critical gap by proposing a framework that enables the concurrent learning of multiple concepts, allowing each concept to aid in the learning of others [20]. Beyond mitigating catastrophic forgetting, this joint learning approach fosters mutual knowledge transfer between concepts, enhancing overall learning efficiency and improving the quality of multi-concept personalization.

Most vision-language problems are instance-based, typically involving the mapping of a fixed-dimensional input tensor to a corresponding target value. However, multi-concept learning can be better formulated as a set-input problem [22], where the input consists of a set of concepts or reference images, and the goal is to generate a corresponding output for the entire set. Effectively addressing this requires treating multi-concept learning within the framework of set-based modeling. A model designed for set-input problems must satisfy two key properties: (1) **permutation invariance**, meaning that the model’s output should remain unchanged regardless of the order in which input elements are presented, and (2) **scalability**, ensuring

that the model can handle input sets of varying sizes without requiring retraining. Building upon these principles, this paper introduces a novel approach to multi-concept learning that jointly learns from multiple concepts while adhering to these fundamental properties.

Specifically, the contributions of this paper are as follows:

1. We propose a two-step joint / parallel learning framework - **Forget Less by Learning Together (FL2T)** - using a text-to-image diffusion model, where we offer flexibility in the order of concept inflow.
2. Utilizing the permutation invariance property of transformers, we develop a concept interaction module that uses proxy embeddings to help alleviate catastrophic forgetting. Additionally, FL2T also accounts for scalability, showing improved performance over SOTA methods with fewer parameters and fewer reference images.

2. Related Work

Continual learning for generative models. For VAEs, Ye, Bors [46, 47] propose online cooperative memorization and continual generative knowledge distillation to mitigate forgetting. Within diffusion models, Zaj *et al.* [51] provide an early study that benchmarks Continual Learning baselines and reports timestep-dependent forgetting patterns and strong replay variants. Masip *et al.* [28] introduce *generative distillation* tailored to diffusion, improving stability across tasks. Recent works [49] also explore lifelong training settings beyond still images, e.g., lifelong video diffusion from a single stream using experience replay and dynamic architectural expansion for diffusion [48].

Forgetting in personalization/customization. Open-world customization emphasizes that adapting a model to new concepts can induce broad semantic and appearance drift, i.e., forgetting beyond the targeted concepts [21]. In continual customization, *Continual Diffusion (C-LoRA)* [39] adds concepts sequentially with parameter-efficient adapters and explicit self-regularization.

Personalization and multi-concept customization. Foundational personalization methods such as Textual Inversion [7] and DreamBooth [36] adapt large text-to-image models to user-provided subjects from a few sample images. For multi-concept learning and composition, Multi-Concept Customization [20] and Mix-of-Show [10] introduce mechanisms for jointly learning and composing multiple concepts.

Interpretability and intra-concept dynamics in diffusion. Analyses of cross-attention provide tools for understanding concept binding and interference during denoising. Prompt-to-Prompt shows that cross-attention controls spatial grounding and can be edited to localize changes [14],

while DAAM [41] performs token-level attribution in Stable Diffusion. These insights motivate designing mechanisms that preserve per-concept subspaces while supporting compositionality.

Prior work [28, 51] on diffusion CL highlights timestep-dependent forgetting and the utility of distillation/replay; continual customization targets sequential concept addition with adapters [39]. Our approach addresses this intersection by enabling *order-agnostic* concept learning with mechanisms aimed at reducing cross-concept interference while maintaining compositional flexibility.

3. Problem Definition

In light of these challenges, we introduce a problem setting called **Order-agnostic Concept-Incremental Flexible Customization**. Building from CIFIC [5], we consider a setting with a variable order of concept inflow. For our problem statement, we assume that the model learns from an undefined series of text-guided concept customization tasks $T = \{T_g\}_{g=1}^G$, where G denotes the total number of tasks. Each task T_g consists of a dataset $T_g = \{(x_k^g, p_k^g, y_k^g)\}_{k=1}^{n_g}$ where n_g is the number of triplets in the task, x_k^g is an image, p_k^g is a text prompt (e.g., “photo of a [V*] [V_{cat}]”), and $y_k^g \in Y_g$ represents the concept tokens in p_k^g . Similar to CIFIC, our setting also supports diverse customization tasks, including multi-concept generation [54], style transfer [52], and image editing [2]. We define Y_g as the concept space for task g , $Y_g = \bigcup_{k=1}^{n_g} y_k^g$ and C_g represents the number of new concepts introduced in task g . In summary, our problem setting consists of three constraints -

1. **All concepts are distinct** : $Y_g \cap \left(\bigcup_{i=1}^{G-1} Y_i\right) = \emptyset$ indicating that new concepts in task g are distinct from those learned in the other $G - 1$ tasks.
2. **Concepts can be learned in any order** : $T = \{\pi(T_1 \cup T_2 \cup \dots \cup T_G) \mid \pi \in S_G\}$ indicating that T consists of any combination of the G concepts in any order, where S_G denotes the symmetric group of G elements, representing all possible permutations.
3. **No-replay constraint** : No memory storage is allocated to retain training data from past tasks, ensuring purely incremental learning of personalized concepts.

This setting allows models to continuously adapt to new personalization tasks while being exposed to catastrophic forgetting of prior concepts.

4. Background

Despite their excellent generation capabilities, existing Custom Diffusion Models (CDMs) [7, 9, 11, 27] (Refer A.6 for details on CDMs) assume that the number of personalized

concepts remains fixed over time, which is unrealistic in real-world applications where users continuously introduce new concepts. Moreover, these models struggle with *catastrophic forgetting* [33] of previously learned concepts. Recent works [5, 19, 23, 39, 40] have proposed various techniques to address the variability in the number of concepts and catastrophic forgetting. In this paper, we will focus on the SOTA framework CIDM [5].

Concept Consolidation Loss (CCL). Introduced in [5], the main purpose of CCL is to facilitate incremental concept learning for a defined order of concept inflow while mitigating catastrophic forgetting. CCL consists of two aspects: Task-Specific Knowledge (TSP) and Task-Shared Knowledge (TSH).

TSP enhances the discriminative ability of the model towards concepts in an incremental learning setup. It uses an orthogonal subspace regularizer to constrain the LoRA weights of different customization tasks. Given the low-rank weight $\Delta\theta_g = \{\Delta\mathbf{W}_g^l\}_{l=1}^L$ for task g , where l denotes the l -th transformer layer and L is the number of layers, each weight matrix can be factorized as $\Delta\mathbf{W}_g^l = \mathbf{A}_g^l \mathbf{B}_g^l$, where $\mathbf{A}_g^l \in \mathbb{R}^{a \times r}$ represents a low-rank concept subspace and $\mathbf{B}_g^l \in \mathbb{R}^{r \times b}$ is its linear weighting matrix. To regulate orthogonality between subspaces of different tasks, TSP minimizes the constraint \mathcal{R}_1 . On the other hand, TSH captures the semantic patterns that persist across different tasks. It introduces a layer-wise common subspace \mathbf{W}_*^l that is shared across tasks. A learnable projection matrix \mathbf{H}_i^l encodes common semantic attributes, optimized by minimizing reconstruction loss.

$$\mathcal{R}_1 = \sum_{i=1}^{g-1} \sum_{l=1}^L \mathbf{A}_i^l (\mathbf{A}_g^l)^\top \quad (1)$$

$$\mathcal{R}_2 = \sum_{i=1}^g \sum_{l=1}^L \|\Delta\mathbf{W}_i^l - \mathbf{H}_i^l \mathbf{W}_*^l\|_F^2 \quad (2)$$

EWA is the foundation of inferencing where previously trained task learners are preserved with a 0.25% memory overhead compared to the SD-1.5 model [35]. The learned LoRA weights are aggregated based on the semantic relationship between stored concept token embedding ($\hat{\mathbf{e}}$) and current task embedding ($\hat{\mathbf{e}}$) in order to reduce forgetting. The aggregated low-rank weight $\Delta\hat{\mathbf{W}}^l$ in the l -th transformer layer is formulated as:

$$\mathcal{M} = \max(\hat{\mathbf{e}}^l \cdot (\hat{\mathbf{e}}^l)^\top) \quad \Delta\hat{\mathbf{W}}^l = \sum_{i=1}^g \Delta\mathbf{W}_i^l \cdot \psi(\mathcal{M})_i \quad (3)$$

where $\max(\cdot)$ operates along the row axis, and $\psi(\mathcal{M}) = \mathcal{M}^2 / \|\mathcal{M}^2\|_F \in \mathbb{R}^g$ normalizes the semantic relations. Here, $\psi(\mathcal{M})_i$ denotes the i -th element of $\psi(\mathcal{M})$.

Inference. After training and applying Eq. 3 to aggregate the learned low-rank weights, we obtain the updated denoising UNet $\epsilon_{\theta'_*}(\cdot)$ for inference, where $\theta'_* = \theta_0 + \Delta\theta_*$ and $\Delta\theta_* = \{\Delta\hat{\mathbf{W}}^l\}_{l=1}^L$. This formulation effectively consolidates the essential characteristics of all personalized concepts.

5. Forget Less by Learning Together (FL2T)

We now present FL2T, a two-step training approach to personalizing diffusion models without the semantic loss of concepts. In the first step, we independently train G different models, where G is the number of concepts. Then, we consolidate all concepts into a single model, leveraging inter-concept interactions for effective personalization.

As in [5], to adapt the g -th text-conditioned concept customization task T_g , we employ Low-Rank Adaptation (LoRA) [15, 45] to fine-tune the pretrained denoising UNet, commonly denoted using ϵ . We define our pretrained UNet model, $\epsilon_{\theta_0}(\cdot)$, to operate on a set of personalized samples $\{\mathbf{x}_g^k, \mathbf{p}_g^k, \mathbf{y}_g^k\}_{k=1}^{n_g}$. Recall that n_g is the number of triplets in the task, x_g^k is an image, p_g^k is a text prompt (e.g., “photo of a [V*] [V_{cat}.]”), and $y_g^k \in Y_g$ represents the concept tokens in p_g^k . The model is trained on these samples to yield an updated model $\epsilon_{\theta'_g}(\cdot)$, where θ'_g is obtained by modifying the base parameters θ_0 with task-specific updates, $\Delta\theta_g$: $\theta'_g = \theta_0 + \Delta\theta_g$. The task-specific update $\Delta\theta_g = \{\Delta\mathbf{W}_g^l\}_{l=1}^L$ consists of low-rank weight modifications for the l -th transformer layer. We know that, from Sec 4, $\Delta\mathbf{W}_g^l \in \mathbb{R}^{a \times b}$ is factorized as $\mathbf{A}_g^l \mathbf{B}_g^l$, with $\mathbf{A}_g^l \in \mathbb{R}^{a \times r}$ and $\mathbf{B}_g^l \in \mathbb{R}^{r \times b}$. As demonstrated in prior research [15, 45], with these adjustments, $\Delta\theta_g$ can encode the distinct characteristics of the personalized concept C_g for task g .

Solutions to our problem setting have been partly addressed in [5, 19, 23, 39, 40]. Although these works reduce catastrophic forgetting, they all operate under a single-umbrella assumption that the order of concepts for customization tasks is fixed. Additionally, to the best of our knowledge, no work uses inter-concept interactions positively. To this end, we propose a novel framework that allows an order-agnostic incremental concept learning and uses inter-concept interactions positively to mitigate catastrophic forgetting.

In order to achieve an optimal order-agnostic continual learning framework, we leverage two intrinsic properties of attention: (1) **permutation invariance / set-invariance**, and (2) **ability to effectively capture higher-order interactions**. Set transformers, introduced in [22], have been used to encode pairwise or higher-order interactions between the elements of a set-invariant input. For an input set of n d -dimensional observations, the Set Transformer combines attention over the d input dimensions with nonlinear functions of pairwise interactions between the input obser-

vations. Further, we have also elucidated a detailed study describing the number of higher-order interactions captured by multiple-layers of attention in Sec. A.4 and Table 7.

Additionally, a theoretical study on the drift of model weights showcases that FL2T (Ours) can achieve a lower model drift (see Sec. A.5). We begin by analyzing one-step model drift when aggregating per-concept gradients $\{m_i\}_{i=1}^G$ either by uniform summation (CIDM: $M_{\text{CIDM}} = \sum_i m_i$) (where M denotes the model parameters) or by unnormalized attention weights (FL2T: $M_{\text{FL2T}} = \sum_i \lambda_i m_i$ with $\lambda_i \in [-1, 1]$). Lemma A.1 establishes a universal upper bound: $\|M_{\text{FL2T}}\| \leq \sum_i \|\lambda_i\|$ which agrees with the worst-case drift of uniform summation and holds for any choice of λ_i in $[-1, 1]$.

Then Theorem A.1 shows that whenever $M_{\text{CIDM}} \neq 0$, one can choose some coefficients (not all equal to 1) so that $\|M_{\text{FL2T}}\| < \|M_{\text{CIDM}}\|$. The constructive proof selects a concept g whose gradient is positively aligned with the aggregate and slightly down-weights it by a small $\varepsilon > 0$, reducing the norm of the update. Intuitively, unnormalized attention performs geometry-aware reweighting that allows cancellation of dominant components of M_{CIDM} , thus consolidating concepts while producing smaller parameter drift per step. When $M_{\text{CIDM}} = 0$, drift is already minimal.

This result formalizes why **attention-based aggregation** is a principled mechanism for our concept consolidation. It **attains lower update magnitude than uniform summation** while preserving flexibility to emphasize or de-emphasize individual concepts, mirroring ideas in multi-objective optimization about mitigating destructive interference between objectives.

5.1. Independent Concept Training (Step 1)

FL2T builds on the key empirical assumption that the concept inflow in Customized Diffusion Models (CDMs) is order-agnostic based on the problem setting in Sec 3. We begin by training each model M_i on its respective task T_i where $i \in [1, G]$. This helps each model learn a stable concept embedding C_g , capturing all semantics relevant to task T_g .

5.2. Concept Aggregation (Step 2)

Recent works [5, 19, 23, 39, 40] have all proposed methods to reduce inter-concept interaction, assuming that the interaction is harmful and can cause the overwriting of concepts. We hypothesise that this inter-concept interaction can rather catalyse generation abilities of concepts and reduce catastrophic forgetting.

Consider the set of concepts to be a directed graph where an edge from concept A to B symbolizes relevant information for B contained within A and vice versa. We define our goal as learning this relevance weight for set-invariant concepts. There are two challenges associated with achieving

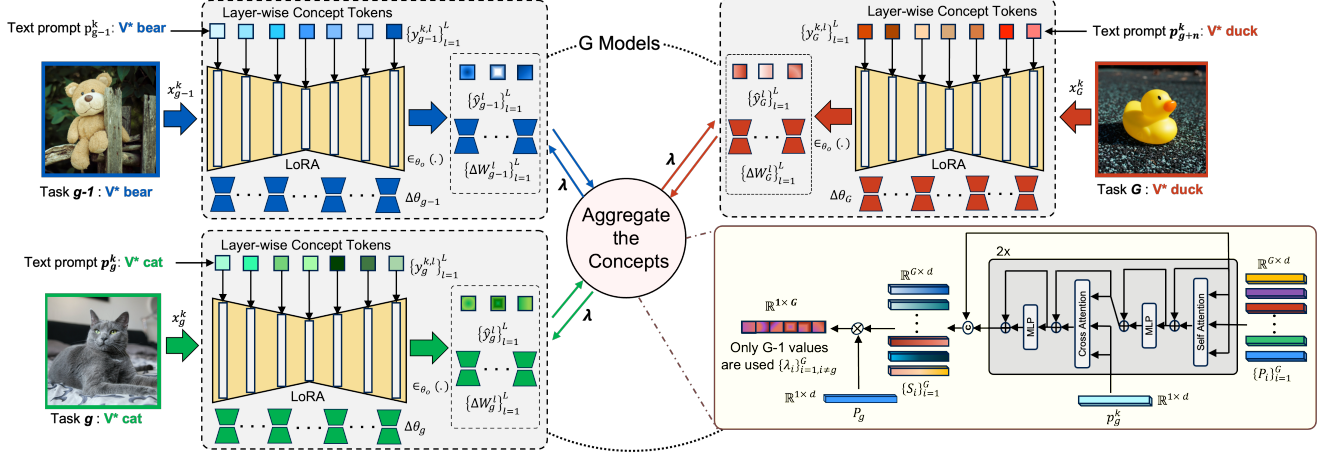


Figure 2. **FL2T overview.** We begin by independently training G models on G concepts for one epoch. Subsequently, in the second epoch, we utilize the learnt concept embeddings (from epoch one) across all concepts to perform cross-concept interactions or aggregate the concepts. To perform these interactions, we use the proxies (initialized with concept embeddings from epoch one) and two transformer layers. The goal of using transformer layers is to capture higher-order interactions between the concept embeddings, g -th concept embedding, and input prompt for task g . Subsequently, we compute a similarity matrix through matrix multiplication to weight the inter-concept interaction. This framework allows variable order of concept inflow, mitigates catastrophic forgetting, and outperforms SOTA frameworks with fewer parameters and fewer reference images.

this, (1) the relevance weights change based on the input prompt, and (2) input data of other concepts is inaccessible. To this end, we utilize learnable embeddings to capture the relevance weights between concepts. These learnable embeddings $\{\mathbf{P}_i\}_{i=1}^G$, also known as proxy embeddings, are initialized with stable concept embeddings $\{\mathbf{C}_i\}_{i=1}^G$ learned in Step 1.

Motivated by the properties of attention in providing permutation invariance, higher-order interactions and lower model-drift, we propose to use transformer decoders for our order-agnostic (set-invariant) framework. The transformer decoder module intends to capture the relevance weights (higher-order interactions) between concepts through proxy embeddings.

Transformer decoders [42] consist of two main blocks: self-attention and cross-attention. The proxy embeddings $\{\mathbf{P}_i\}_{i=1}^G$ serve as input to the decoder that first performs self-attention. Subsequently, it is cross-attended with input text-prompt for task g , outputting $\{\mathbf{P}'_i\}_{i=1}^G$. The objective of this is to capture the relevance scores between concepts for a particular text prompt. Although transformers are adept at capturing higher-order interactions, they are also susceptible to rank collapse [18].

To address this rank collapse, we introduce two things: (1) a non-linear transformation layer such as an MLP, and (2) contrastive loss. The attended proxy embeddings $\{\mathbf{P}'_i\}_{i=1}^G$ are combined with the original concept embeddings: $S_i = \{f(\mathbf{C}_i | \mathbf{P}'_i)\}_{\forall i \neq g}$, where $f(\cdot | \cdot)$ represents a non-linear transformation such as an MLP on two concatenated vectors. On the other hand, the contrastive loss con-

strains embeddings to be distinct and away from each other in terms of cosine distance while ensuring they capture relevant information. It is applied on $\{S_i\}_{i=1}^G$ as given in Eq. 4 where $\text{sim}(\mathbf{z}_i, \mathbf{z}_j) = \frac{\mathbf{z}_i \cdot \mathbf{z}_j}{\|\mathbf{z}_i\| \|\mathbf{z}_j\|}$ and τ is the temperature hyperparameter.

$$\mathcal{R}_3 = \frac{1}{G} \sum_{i=1}^G -\log \frac{\exp(\text{sim}(S_i, S_i)/\tau)}{\sum_{j=1}^N \exp(\text{sim}(S_i, S_j)/\tau)} \quad (4)$$

Recall that in Sec 4, we introduced Task-Specific Knowledge that regulates orthogonality between subspaces of different tasks. Here, we extend that by weighting the constraint with relevance weights between concepts depending on the input prompt \mathbf{p}_g^k :

$$\mathcal{R}'_1 = \sum_{i=1, i \neq g}^G \sum_{l=1}^L \lambda_i \mathbf{A}_i^l (\mathbf{A}_g^l)^\top \quad (5)$$

where λ is the edge weight derived through proxy embeddings for each concept g . For a given task T_g , we compute the importance weights $\{\lambda_i\}_{i=1, i \neq g}^G$ by measuring the similarity between the concept embedding \mathbf{C}_g and the transformed representations \mathbf{S}_i that has captured the higher-order interactions of concepts: $\lambda_i = \{\mathbf{C}_g \mathbf{S}_i^\top\}_{\forall i \neq g}$. This formulation enables the selection of the most relevant concepts for each task.

Finally, from Sec 4, we define the loss function as:

$$\mathcal{L} = \mathcal{E}_{z \sim E(x_g^k), c_g^k, \epsilon \sim \mathcal{N}(0, I), t} \left[\left\| \epsilon - \epsilon_{\theta'_g}(z_t | c_g^k, t) \right\|_2^2 + \mathcal{R}'_1 + \gamma_1 \mathcal{R}_2 + \gamma_2 \mathcal{R}_3 \right] \quad (6)$$

where $c_g^k = \{c_g^{k,l}\}_{l=1}^L$ represents layer-wise textual embeddings, and γ is the trade-off hyperparameter.

6. Experiments

We train FL2T on three datasets - CIFC [5], CelebA [26] and ImageNet [4], each consisting of ten distinct concepts with 3-5 text-image pairs. We follow the evaluation strategy defined in [5]. Specifically, twenty evaluation prompts are introduced for each of the ten concepts, and fifty images are generated per prompt. More information on datasets, hyperparameters and evaluation metrics has been provided in the Appendix.

6.1. Ablation Studies

This section analyzes the effect of our proxy-guided concept aggregation module on the variation in the number of LoRA parameters, number of transformer layers, and number of reference images.

On the number of reference images. We further compare CIDM [5] and FL2T (Ours) by imposing a constraint on the number of reference images while evaluating both models on the same prompts as the original dataset, as shown in Fig. 3(a). As expected, the performance of both models improves linearly with an increasing number of reference images. However, FL2T consistently outperforms CIDM across all cases and achieves performance comparable to CIDM on the original dataset (≥ 4 images) with only three reference images, highlighting the efficiency and effectiveness of our approach. *FL2T performs better than SOTA models with fewer reference images.*

Number of transformer decoder layers. As shown in Table 2, the proxy embeddings achieve optimal inter-concept semantic representation with two transformer layers. This can be attributed to the tendency of excessive attention layers to induce rank collapse, leading to a rank-1 matrix and reduced representational diversity [18]. On the other hand, a single transformer layer is too small to capture feature relations. *FL2T achieves maximal performance with two transformer decoder layers.*

Variation of LoRA parameters. Fig. 3(b) and Table 4 illustrate the impact of varying LoRA parameters on model performance. Across all ranks of the LoRA matrix, FL2T (Ours) consistently outperforms CIDM [5] across all scores. Notably, our framework achieves superior performance compared to CIDM (rank = 4) while utilizing a lower

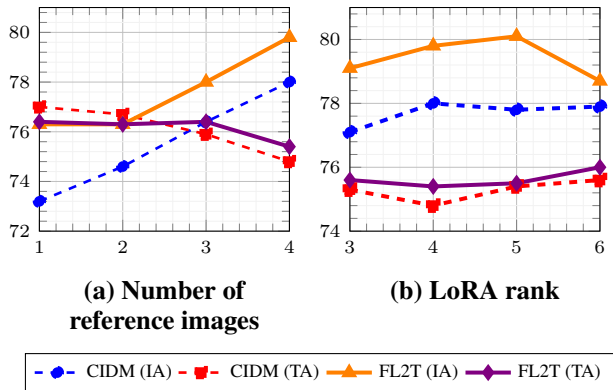


Figure 3. **Ablation studies.** We compare the performance of FL2T against CIDM: with a constraint on the (a) number of reference images, and (b) on the LoRA rank. In each case, FL2T exhibits superior performance.

rank or 25% fewer parameters. *FL2T exhibits greater parameter efficiency by outperforming SOTA models while using a lower LoRA rank.*

On the number of concepts. As shown in Fig. 4, FL2T (Ours) exhibits impressive scalability compared to CIDM [5]. This further consolidates our hypothesis that positive inter-concept interactions can help improve generative capabilities. *FL2T demonstrates impressive scalability.*

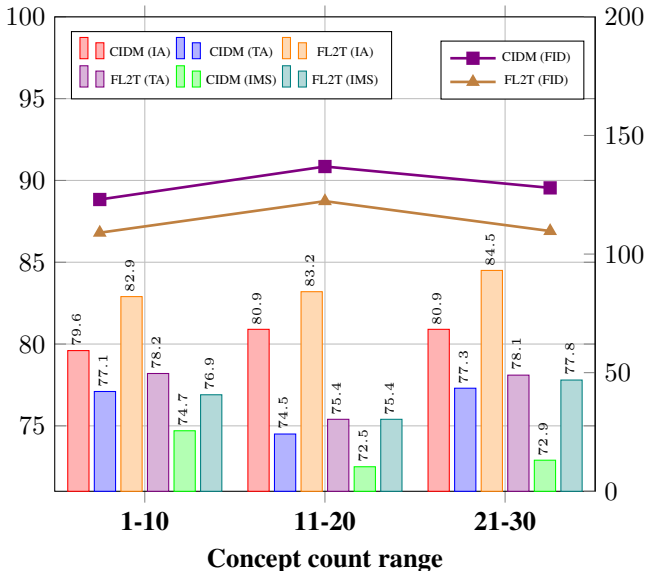


Figure 4. **Scalability.** FL2T shows impressive scalability achieving higher average CLIP and IMS scores (left axis) and lower FID values (right axis) over three concept ranges (1–10, 11–20, 21–30), compared to CIDM [5] on the ImageNet dataset [4]. We limit the scalability analysis to 30 concepts due to CLIP tokenizer’s limit on 77 new tokens.

Methods	V1		V2		V3		V4		V5		V6		V7		V8		V9		V10		Avg.		
	IA	TA	IA	TA	IA	TA	IA	TA	IA	TA	IA	TA	IA	TA	IA	TA	IA	TA	IA	TA	IA	TA	
CIFC [5]	Previous frameworks																						
	Finetuning	77.6	64.4	82.2	74.6	79.0	69.4	77.6	68.6	79.6	75.0	62.9	70.0	71.5	<u>76.7</u>	53.7	69.2	81.4	65.4	72.1	67.2	73.7	70.0
	EWC [19]	78.7	67.1	83.8	77.5	80.4	72.7	80.3	77.9	80.7	76.7	64.0	72.3	76.5	74.2	57.1	72.0	84.4	66.0	73.1	70.4	75.9	72.7
	LWF [23]	80.4	70.8	79.7	75.2	80.9	71.0	77.4	77.4	80.9	76.0	61.8	71.7	73.2	76.3	53.5	72.9	78.1	72.5	74.7	70.0	74.1	73.4
	CLoRA [39]	83.2	69.4	83.4	78.0	81.1	74.1	80.6	78.8	84.9	76.4	66.3	69.6	76.2	<u>76.7</u>	58.1	73.9	83.0	69.0	72.1	71.8	76.9	73.6
	L2DM [40]	78.7	68.6	86.3	79.5	76.6	70.1	80.7	73.0	86.8	76.7	70.8	67.7	70.0	75.9	59.3	74.1	77.7	71.8	74.1	69.4	76.1	72.7
	On the effectiveness of concept aggregation																						
	Ours w/o guidance	82.4	<u>76.1</u>	83.9	<u>82.5</u>	80.9	74.9	78.8	<u>82.5</u>	84.6	<u>79.8</u>	66.0	<u>74.2</u>	82.9	73.7	59.8	76.3	81.8	73.4	75.6	71.6	77.7	<u>76.5</u>
	Ours with Cosine-guidance	81.8	74.8	84.6	82.2	80.1	<u>75.9</u>	77.9	81.3	85.2	79.2	76.7	72.0	83.9	72.3	59.3	77.1	82.2	73.4	76.7	<u>72.2</u>	78.8	76.0
	Comparison against SOTA framework																						
	CIDM [5]	83.6	75.3	86.4	78.1	82.9	74.0	80.8	81.1	86.5	78.2	69.5	70.1	73.7	74.7	56.9	74.3	82.4	73.5	75.9	70.2	78.0	74.8
	Ours with proxy-guidance	84.4	74.0	86.1	81.6	84.4	70.1	82.2	81.1	87.2	78.0	69.3	72.9	85.3	70.4	60.7	<u>77.6</u>	82.1	<u>76.6</u>	76.5	71.6	79.8	<u>75.4</u>
	Δ	+0.8	-1.3	-0.3	+3.5	+1.5	-4.0	+1.4	+0.0	+0.7	-0.2	-1.5	+0.6	+9.2	-6.3	+1.4	+3.3	-2.3	+3.1	+0.6	-0.2	+1.8	+0.6
	CelebA [26]	Comparison against SOTA framework																					
		CIDM [5]	74.2	<u>59.0</u>	67.6	60.4	73.0	59.4	75.4	58.2	70.1	58.0	78.1	59.0	81.0	58.4	70.0	58.0	70.1	62.1	73.0	55.4	73.3
Ours with proxy-guidance		76.4	58.9	72.7	<u>60.7</u>	73.1	<u>60.0</u>	77.2	<u>63.0</u>	78.1	<u>61.5</u>	80.0	<u>60.9</u>	83.4	<u>60.6</u>	72.0	<u>63.1</u>	73.1	<u>62.7</u>	74.5	<u>57.9</u>	76.1	<u>60.9</u>
Δ		+2.2	-0.1	+5.1	+0.3	+0.1	+0.6	+1.8	+4.8	+8.0	+3.5	+1.9	+1.9	+2.4	+2.2	+2.0	+5.1	+3.0	+0.6	+1.5	+2.5	+2.8	+2.1
ImageNet [4]	Comparison against SOTA framework																						
	CIDM [5]	80.8	74.1	71.4	<u>77.9</u>	81.3	<u>81.7</u>	83.0	82.6	79.2	<u>83.7</u>	84.5	69.6	76.7	72.3	87.5	73.7	82.2	79.9	85.0	82.8	81.2	78.5
	Ours with proxy-guidance	83.3	<u>74.8</u>	75.7	73.1	82.1	79.8	84.4	<u>83.3</u>	83.3	<u>83.7</u>	84.8	<u>70.2</u>	78.7	<u>73.9</u>	88.1	<u>77.5</u>	83.3	<u>80.2</u>	92.6	<u>86.8</u>	83.7	<u>79.0</u>
	Δ	+2.5	+0.7	+4.3	-4.8	+0.8	-1.9	+1.4	+0.7	+4.1	+0.0	+0.3	+0.6	+2.0	+1.6	+0.6	+3.8	+1.1	+0.3	+7.6	+4.0	+2.5	+0.5

Table 1. **Quantitative Analysis.** We compare our method, denoted by ‘‘Ours with proxy-guidance’’ against SOTA frameworks, observing an improvement in both IA and TA scores in at least 6 out of 10 concepts. Further experimentation with uncontrolled (‘‘Ours w/o guidance’’) and cosine-similarity (‘‘Ours with Cosine-guidance’’) based inter-concept interactions showcase the need for proxy-guidance on the interactions. IA and TA refer to CLIP [32] Image Alignment and Text Alignment scores respectively.

Number of layers	V1 - V5		V6 - V10		Avg.	
	IA (↑)	TA (↑)	IA (↑)	TA (↑)	IA (↑)	TA (↑)
1	83.5	77.3	73.4	<u>74.1</u>	78.5	<u>75.7</u>
2	84.9	77.0	74.8	73.8	79.8	75.4
3	84.9	76.8	74.0	73.7	79.4	75.3
4	83.7	<u>77.6</u>	73.4	72.7	78.6	75.2
Number of layers	IMS (↑)	FID (↓)	IMS (↑)	FID (↓)	IMS (↑)	FID (↓)
1	75.3	139.8	63.4	262.7	69.4	201.2
2	78.2	133.3	64.4	262.7	71.3	198.0
3	77.3	<u>132.2</u>	63.7	<u>261.0</u>	70.5	<u>196.6</u>
4	76.5	139.3	62.9	265.2	69.7	202.3

Table 2. Comparison of model performances based on the number of transformer layers in the concept aggregation module. The best IA and IMS scores have been denoted in **bold**, and TA and FID values have been underlined.

6.2. Quantitative Analysis

As shown in Table 1, we begin our experiments by evaluating our framework under the condition where 9 out of 10 concepts are exposed for a task g , referred to as ‘‘Ours w/o guidance.’’ We then introduce cosine similarity-based guidance to regulate cross-concept interactions using the concept embeddings learned in Step 1 (Section 5.1), which is denoted as ‘‘Ours with Cosine-guidance.’’ This adjustment

leads to a notable improvement of +0.8 in the average Image Alignment (IA) scores, with only a negligible decrease in the average Text Alignment (TA) scores. Notably, Concept V6 experiences a substantial 10-point improvement in IA scores. Inspired by this observation, we designed a module that controls cross-concept interactions using proxy embeddings. The results demonstrate that our framework outperforms CIDM [5] in at least 6 out of 10 concepts across both IA and TA scores. The smallest gain observed is +0.6, while the largest gain is +9.2. Furthermore, our framework effectively supports the paradigm of personalization and mitigates catastrophic forgetting, as evidenced by a +1.8 improvement in average IA scores and +0.6 in average TA scores. We would also like to highlight the fact that FL2T showcases superior performance in terms of LoRA parameter efficiency (Fig. 3 (b)) and fewer reference images required for optimal performance (Fig. 3(a)).

6.3. Qualitative Analysis

As demonstrated in Fig. 5, our proposed framework excels in preserving identity, evidenced by the V7 concept generation task. It is also adept at controlling the number of objects in the generated images, as shown in V1 dog and



Figure 5. Qualitative Analysis on the CIFC dataset [5]. We compare the synthesized images by CIDM [5] and FL2T (Ours). The images are generated with a source image and an associated text prompt as input. Images with red and green arrows indicate regions of undesirable and desirable qualities, and their reasons are stated below each image.

V8 drawing concept images (Appendix Fig. 9). Lastly, we also observe a substantial improvement in correcting extraneous features and background generation capabilities. We attribute this improvement to the effective cross-concept interactions, which lead to the generation of more robust concept embeddings. Furthermore, the use of proxy-guidance aids in achieving smoother knowledge transfer and retention across concepts, as illustrated by the enhanced quality of the generated images.

6.4. Computational Cost Analysis

We evaluate the computational efficiency of our method by comparing the parameter count, time complexity, memory consumption, and inference latency against CIDM [5]. FL2T (Ours) has a higher parameter count (52.6M) compared to CIDM [5] (38.4M), due to its proxy-guided inter-concept interaction architecture. Our method exhibits improved performance with a time complexity of $\mathcal{O}(2G)$, compared to CIDM’s $\mathcal{O}(G)$, where G is the number of concepts. Both methods exhibit identical memory consumption of 18.7 GB during inference. Additionally, the inference times for processing 50 images are comparable: 1423 seconds for CIDM and 1436 seconds for FL2T, highlighting that the increased parameter count does not lead to a substantial increase in runtime.

7. Limitations

Despite its strengths, FL2T exhibits a few limitations. First, it occasionally fails to accurately generate the prompted context, which can be attributed to weak priors for certain concepts or low co-occurrence between the subject and context in the training data (e.g., as seen in row 2, column 6 of Fig. 5). Second, the model may overfit to real images when the prompt closely mirrors conditions seen during training, limiting its generalization. Lastly, FL2T’s ability to learn subject identities varies significantly - while common subjects such as dogs and cats are modeled effectively, rare or less-represented subjects remain challenging.

8. Conclusion

Our work tackles the limitations of existing CDMs, particularly their susceptibility to catastrophic forgetting when learning new concepts. Unlike prior approaches that assume a fixed order of concept learning and neglect inter-concept interactions, we introduce Forget Less by Learning Together (FL2T) — a novel framework that enables order-agnostic concept learning while mitigating forgetting. At the core of FL2T is an inter-concept learning mechanism which leverages the permutation invariance property of transformers. In this mechanism, proxy embeddings guide feature selection across concepts, ensuring both knowledge retention and efficient adaptation. By leveraging inter-concept guidance, our method preserves previously learned concepts while seamlessly integrating new ones.

References

- [1] Hila Chefer, Yuval Alaluf, Yael Vinker, Lior Wolf, and Daniel Cohen-Or. Attend-and-excite: Attention-based semantic guidance for text-to-image diffusion models. *ACM Trans. Graph.*, 42(4), July 2023. [15](#)
- [2] Xi Chen, Lianghua Huang, Yu Liu, Yujun Shen, Deli Zhao, and Hengshuang Zhao. AnyDoor: Zero-shot Object-level Image Customization. In *IEEE/CVF Conference on Computer Vision and Pattern Recognition (CVPR)*, pages 6593–6602, Los Alamitos, CA, USA, June 2024. IEEE Computer Society. [3](#)
- [3] Jun Cheng, Fuxiang Wu, Yanling Tian, Lei Wang, and Dapeng Tao. Rifegan: Rich feature generation for text-to-image synthesis from prior knowledge. In *IEEE/CVF Conference on Computer Vision and Pattern Recognition (CVPR)*, pages 10908–10917, 2020. [1](#)
- [4] Jia Deng, Wei Dong, Richard Socher, Li-Jia Li, Kai Li, and Li Fei-Fei. Imagenet: A large-scale hierarchical image database. In *IEEE Conference on Computer Vision and Pattern Recognition*, pages 248–255, 2009. [6](#), [7](#), [12](#), [13](#), [15](#), [16](#)
- [5] Jiahua Dong, Wenqi Liang, Hongliu Li, Duzhen Zhang, Meng Cao, Henghui Ding, Salman Khan, and Fahad Shahbaz Khan. How to continually adapt text-to-image diffusion models for flexible customization? In *Proceedings of the 38th International Conference on Neural Information Processing Systems, NIPS*, Red Hook, NY, USA, 2024. Curran Associates Inc. [1](#), [2](#), [3](#), [4](#), [6](#), [7](#), [8](#), [12](#), [13](#), [14](#), [15](#), [16](#), [17](#)
- [6] Yutong Feng, Biao Gong, Di Chen, Yujun Shen, Yu Liu, and Jingren Zhou. Ranni: Taming text-to-image diffusion for accurate instruction following. In *IEEE/CVF Conference on Computer Vision and Pattern Recognition (CVPR)*, pages 4744–4753, 2024. [1](#)
- [7] Rinon Gal, Yuval Alaluf, Amit H. Bermano, Gal Chechik, Daniel Cohen-Or, and Tali Dekel Gal. An image is worth one word: Personalizing text-to-image generation using textual inversion. In *ICLR*, 2023. [1](#), [2](#), [3](#), [15](#)
- [8] Shuyang Gu, Dong Chen, Jianmin Bao, Fang Wen, Bo Zhang, Dongdong Chen, Lu Yuan, and Baining Guo. Vector quantized diffusion model for text-to-image synthesis. In *IEEE/CVF Conference on Computer Vision and Pattern Recognition (CVPR)*, pages 10686–10696, 2022. [15](#)
- [9] Yuchao Gu, Xintao Wang, Jay Zhangjie Wu, Yujun Shi, Yunpeng Chen, Zihan Fan, Wuyou Xiao, Rui Zhao, Shuning Chang, Weijia Wu, Yixiao Ge, Ying Shan, and Mike Zheng Shou. Mix-of-show: decentralized low-rank adaptation for multi-concept customization of diffusion models. In *Proceedings of the 37th International Conference on Neural Information Processing Systems, NIPS*, Red Hook, NY, USA, 2023. Curran Associates Inc. [2](#), [3](#), [15](#)
- [10] Yuchao Gu, Xintao Wang, Jay Zhangjie Wu, Yujun Shi, Yunpeng Chen, Zihan Fan, Wuyou Xiao, Rui Zhao, Shuning Chang, Weijia Wu, Yixiao Ge, Ying Shan, and Mike Zheng Shou. Mix-of-show: Decentralized low-rank adaptation for multi-concept customization of diffusion models. In *NeurIPS*, 2023. [2](#)
- [11] Ligong Han, Yinxiao Li, Han Zhang, Peyman Milanfar, Dimitris Metaxas, and Feng Yang. Svdif: Compact parameter space for diffusion fine-tuning. In *IEEE/CVF International Conference on Computer Vision (ICCV)*, pages 7289–7300, 2023. [3](#), [15](#)
- [12] Shaozhe Hao, Kai Han, Shihao Zhao, and Kwan-Yee K. Wong. Vico: Plug-and-play visual condition for personalized text-to-image generation, 2023. [2](#)
- [13] Kaiming He, Xiangyu Zhang, Shaoqing Ren, and Jian Sun. Deep residual learning for image recognition. In *2016 IEEE Conference on Computer Vision and Pattern Recognition (CVPR)*, pages 770–778, 2016. [12](#)
- [14] Amir Hertz, Ron Mokady, Jay Tenenbaum, Kfir Aberman, Yael Pritch, and Daniel Cohen-Or. Prompt-to-prompt image editing with cross-attention control. In *International Conference on Learning Representations (ICLR)*, 2023. [2](#)
- [15] Edward J Hu, Yelong Shen, Phillip Wallis, Zeyuan Allen-Zhu, Yuanzhi Li, Shean Wang, Lu Wang, and Weizhu Chen. LoRA: Low-rank adaptation of large language models. In *International Conference on Learning Representations (ICLR)*, 2022. [4](#), [12](#), [15](#)
- [16] Phillip Isola, Jun-Yan Zhu, Tinghui Zhou, and Alexei A. Efros. Image-to-image translation with conditional adversarial networks. In *IEEE Conference on Computer Vision and Pattern Recognition (CVPR)*, pages 5967–5976, 2017. [15](#)
- [17] Sadeep Jayasumana, Srikumar Ramalingam, Andreas Veit, Daniel Glasner, Ayan Chakrabarti, and Sanjiv Kumar. Re-thinking fid: Towards a better evaluation metric for image generation. In *IEEE/CVF Conference on Computer Vision and Pattern Recognition (CVPR)*, pages 9307–9315, 2024. [13](#), [14](#)
- [18] Jihwan Kim, Miso Lee, Cheol-Ho Cho, Jihyun Lee, and Jae-Pil Heo. Prediction-feedback detr for temporal action detection. In *Proceedings of the Thirty-Ninth AAAI Conference on Artificial Intelligence and Thirty-Seventh Conference on Innovative Applications of Artificial Intelligence and Fifteenth Symposium on Educational Advances in Artificial Intelligence, AAAI/IAAI/EAAI*. AAAI Press, 2025. [5](#), [6](#), [12](#)
- [19] James Kirkpatrick, Razvan Pascanu, Neil Rabinowitz, Joel Veness, Guillaume Desjardins, Andrei A. Rusu, Kieran Milan, John Quan, Tiago Ramalho, Agnieszka Grabska-Barwinska, Demis Hassabis, Claudia Clopath, Dharshan Kumaran, and Raia Hadsell. Overcoming catastrophic forgetting in neural networks. *Proceedings of the National Academy of Sciences*, 114(13):3521–3526, Mar. 2017. [3](#), [4](#), [7](#)
- [20] Nupur Kumari, Bohan Zhang, Richard Zhang, Eli Shechtman, and Jun-Yan Zhu. Multi-concept customization of text-to-image diffusion. In *IEEE/CVF Conference on Computer Vision and Pattern Recognition (CVPR)*, pages 1931–1941, 2023. [2](#), [13](#), [14](#), [15](#)
- [21] Héctor Laria, Alex Gomez-Villa, Kai Wang, Bogdan Raducanu, and Joost van de Weijer. Assessing open-world forgetting in generative image model customization. *arXiv preprint arXiv:2410.14159*, 2024. [2](#)

- [22] Juho Lee, Yoonho Lee, Jungtaek Kim, Adam Kosior, Seungjin Choi, and Yee Whye Teh. Set transformer: A framework for attention-based permutation-invariant neural networks. In Kamalika Chaudhuri and Ruslan Salakhutdinov, editors, *Proceedings of the 36th International Conference on Machine Learning*, volume 97 of *Proceedings of Machine Learning Research*, pages 3744–3753. PMLR, 09–15 Jun 2019. 2, 4
- [23] Zhizhong Li and Derek Hoiem. Learning without forgetting. *IEEE Trans. Pattern Anal. Mach. Intell.*, 40(12):2935–2947, Dec. 2018. 3, 4, 7
- [24] Chang Liu, Xiangtai Li, and Henghui Ding. Referring image editing: Object-level image editing via referring expressions. In *IEEE/CVF Conference on Computer Vision and Pattern Recognition (CVPR)*, pages 13128–13138, 2024. 1
- [25] Yixin Liu, Chenrui Fan, Yutong Dai, Xun Chen, Pan Zhou, and Lichao Sun. Metacloak: Preventing unauthorized subject-driven text-to-image diffusion-based synthesis via meta-learning. In *IEEE/CVF Conference on Computer Vision and Pattern Recognition (CVPR)*, pages 24219–24228, 2024. 12, 13, 14
- [26] Ziwei Liu, Ping Luo, Xiaogang Wang, and Xiaoou Tang. Deep learning face attributes in the wild. In *Proceedings of International Conference on Computer Vision (ICCV)*, December 2015. 6, 7, 12, 13, 15, 16
- [27] Zhiheng Liu, Yifei Zhang, Yujun Shen, Kecheng Zheng, Kai Zhu, Ruili Feng, Yu Liu, Deli Zhao, Jingren Zhou, and Yang Cao. Cones 2: customizable image synthesis with multiple subjects. In *Proceedings of the 37th International Conference on Neural Information Processing Systems*, NIPS, Red Hook, NY, USA, 2023. Curran Associates Inc. 3, 15
- [28] Sergi Masip, Pau Rodríguez, Tinne Tuytelaars, and Gido M. van de Ven. Continual learning of diffusion models with generative distillation. In *Proceedings of the Conference on Lifelong Learning Agents (CoLLAs)*, volume 274 of *PMLR*, pages 431–456, 2024. 2, 3
- [29] Ron Mokady, Amir Hertz, Kfir Aberman, Yael Pritch, and Daniel Cohen-Or. Null-text inversion for editing real images using guided diffusion models. In *IEEE/CVF Conference on Computer Vision and Pattern Recognition (CVPR)*, pages 6038–6047, 2023. 1
- [30] Taesung Park, Ming-Yu Liu, Ting-Chun Wang, and Jun-Yan Zhu. Semantic image synthesis with spatially-adaptive normalization. In *IEEE/CVF Conference on Computer Vision and Pattern Recognition (CVPR)*, pages 2332–2341, 2019. 15
- [31] Dustin Podell, Zion English, Kyle Lacey, Andreas Blattmann, Tim Dockhorn, Jonas Müller, Joe Penna, and Robin Rombach. Sdxl: Improving latent diffusion models for high-resolution image synthesis. In B. Kim, Y. Yue, S. Chaudhuri, K. Fragkiadaki, M. Khan, and Y. Sun, editors, *International Conference on Representation Learning*, volume 2024, pages 1862–1874, 2024. 1, 15
- [32] Aditya Ramesh, Prafulla Dhariwal, Alex Nichol, Casey Chu, and Mark Chen. Hierarchical text-conditional image generation with clip latents. *ArXiv*, abs/2204.06125, 2022. 7, 12, 13, 15
- [33] Sylvestre-Alvise Rebuffi, Alexander Kolesnikov, Georg Sperl, and Christoph H. Lampert. icarl: Incremental classifier and representation learning, 2017. 3
- [34] Scott Reed, Zeynep Akata, Xinchun Yan, Lajanugen Logeswaran, Bernt Schiele, and Honglak Lee. Generative adversarial text to image synthesis. In Maria Florina Balcan and Kilian Q. Weinberger, editors, *Proceedings of The 33rd International Conference on Machine Learning*, volume 48 of *Proceedings of Machine Learning Research*, pages 1060–1069, New York, New York, USA, 20–22 Jun 2016. PMLR. 1, 15
- [35] Robin Rombach, Andreas Blattmann, Dominik Lorenz, Patrick Esser, and Bjorn Ommer. High-Resolution Image Synthesis with Latent Diffusion Models. In *IEEE/CVF Conference on Computer Vision and Pattern Recognition (CVPR)*, pages 10674–10685, Los Alamitos, CA, USA, June 2022. IEEE Computer Society. 3, 12, 15
- [36] Nataniel Ruiz, Yuanzhen Li, Varun Jampani, Yael Pritch, Michael Rubinstein, and Kfir Aberman. Dreambooth: Fine tuning text-to-image diffusion models for subject-driven generation. In *IEEE/CVF Conference on Computer Vision and Pattern Recognition (CVPR)*, pages 22500–22510, 2023. 2, 15
- [37] Chitwan Saharia, William Chan, Saurabh Saxena, Lala Lit, Jay Whang, Emily Denton, Seyed Kamyar Seyed Ghasemipour, Burcu Karagol Ayan, S. Sara Mahdavi, Raphael Gontijo-Lopes, Tim Salimans, Jonathan Ho, David J Fleet, and Mohammad Norouzi. Photorealistic text-to-image diffusion models with deep language understanding. In *Proceedings of the 36th International Conference on Neural Information Processing Systems*, NIPS, Red Hook, NY, USA, 2022. Curran Associates Inc. 15
- [38] Sefik Ilkin Serengil and Alper Ozpinar. Hyperextended light-face: A facial attribute analysis framework. In *International Conference on Engineering and Emerging Technologies (ICEET)*, pages 1–4, 2021. 13
- [39] James Seale Smith, Yen-Chang Hsu, Lingyu Zhang, Ting Hua, Zsolt Kira, Yilin Shen, and Hongxia Jin. Continual diffusion: Continual customization of text-to-image diffusion with c-lora. *Transactions on Machine Learning Research (TMLR)*, 2024. 2, 3, 4, 7
- [40] Gan Sun, Wenqi Liang, Jiahua Dong, Jun Li, Zhengming Ding, and Yang Cong. Create your world: Lifelong text-to-image diffusion. *IEEE Transactions on Pattern Analysis and Machine Intelligence*, 46(9):6454–6470, 2024. 3, 4, 7
- [41] Raphael Tang, Linqing Liu, Akshat Pandey, Zhiying Jiang, Gefei Yang, Karun Kumar, Pontus Stenetorp, Jimmy Lin, and Ferhan Ture. What the daam: Interpreting stable diffusion using cross attention. In *ACL*, 2023. 3
- [42] Ashish Vaswani, Noam Shazeer, Niki Parmar, Jakob Uszkoreit, Llion Jones, Aidan N. Gomez, Łukasz Kaiser, and Illia Polosukhin. Attention is all you need. In *Proceedings of the 31st International Conference on Neural Information Processing Systems*, NIPS, page 6000–6010, Red Hook, NY, USA, 2017. Curran Associates Inc. 5
- [43] Boyang Wang, Fengyu Yang, Xihang Yu, Chao Zhang, and Hanbin Zhao. APISR: Anime Production Inspired Real-World Anime Super-Resolution. In *IEEE/CVF Conference*

- on *Computer Vision and Pattern Recognition (CVPR)*, pages 25574–25584, Los Alamitos, CA, USA, June 2024. IEEE Computer Society. [1](#)
- [44] Kai Wang, Fei Yang, Bogdan Raducanu, and Joost van de Weijer. Multi-Class Textual-Inversion Secretly Yields a Semantic-Agnostic Classifier. In *IEEE/CVF Winter Conference on Applications of Computer Vision (WACV)*, pages 4400–4409, Los Alamitos, CA, USA, Mar. 2025. IEEE Computer Society. [1](#)
- [45] Xiao Wang, Tianze Chen, Qiming Ge, Han Xia, Rong Bao, Rui Zheng, Qi Zhang, Tao Gui, and Xuanjing Huang. Orthogonal subspace learning for language model continual learning. In Houda Bouamor, Juan Pino, and Kalika Bali, editors, *Findings of the Association for Computational Linguistics: EMNLP*, pages 10658–10671, Singapore, Dec. 2023. Association for Computational Linguistics. [4](#), [12](#), [15](#)
- [46] Fei Ye and Adrian G. Bors. Continual variational autoencoder learning via online cooperative memorization. In *ECCV*, pages 531–549, 2022. [2](#)
- [47] Fei Ye and Adrian G. Bors. Continual variational autoencoder via continual generative knowledge distillation. In *AAAI Conference on Artificial Intelligence (AAAI)*, volume 37, pages 10918–10926, 2023. [2](#)
- [48] Fei Ye, Adrian G. Bors, and Kun Zhang. Dynamic expansion diffusion learning for lifelong generative modelling. In *AAAI Conference on Artificial Intelligence (AAAI)*, volume 39, pages 22101–22109, 2025. [2](#)
- [49] Jason Yoo, Yingchen He, Saeid Naderiparizi, Dylan Green, Gido M. van de Ven, Geoff Pleiss, and Frank Wood. Lifelong learning of video diffusion models from a single video stream. *arXiv preprint arXiv:2406.04814*, 2024. [2](#)
- [50] Zhengyang Yu, Zhaoyuan Yang, and Jing Zhang. Dreamsteerer: enhancing source image conditioned editability using personalized diffusion models. In *Proceedings of the 38th International Conference on Neural Information Processing Systems, NIPS*, Red Hook, NY, USA, 2024. Curran Associates Inc. [1](#)
- [51] Michał Zajac, Kamil Deja, Anna Kuzina, Jakub M. Tomczak, Tomasz Trzciński, Florian Shkurti, and Piotr Miłoś. Exploring continual learning of diffusion models. *arXiv:2303.15342*, 2023. [2](#), [3](#)
- [52] Yuxin Zhang, Nisha Huang, Fan Tang, Haibin Huang, Chongyang Ma, Weiming Dong, and Changsheng Xu. Inversion-based style transfer with diffusion models. In *IEEE/CVF Conference on Computer Vision and Pattern Recognition (CVPR)*, pages 10146–10156, 2023. [3](#)
- [53] Rui Zhao, Yuchao Gu, Jay Zhangjie Wu, David Junhao Zhang, Jia-Wei Liu, Weijia Wu, Jussi Keppo, and Mike Zheng Shou. Motiondirector: Motion customization of text-to-video diffusion models. In *Computer Vision – ECCV 2024: 18th European Conference, Milan, Italy, September 29–October 4, 2024, Proceedings, Part LVI*, page 273–290, Berlin, Heidelberg, 2024. Springer-Verlag. [15](#)
- [54] Ming Zhong, Yelong Shen, Shuohang Wang, Yadong Lu, Yizhu Jiao, Siru Ouyang, Donghan Yu, Jiawei Han, and Weizhu Chen. Multi-lora composition for image generation, 2024. [3](#)

A. Technical Appendices and Supplementary Material

A.1. Ablation study

We conduct an ablation study comparing FL2T (Ours) and CIDM [5] under varying settings. First, constraining the number of reference images (Table 3) reveals that while both models improve with more references, FL2T consistently outperforms CIDM and matches its original performance (≥ 4 images) using only three, demonstrating greater efficiency. Second, as shown in Table 2 proxy embeddings attain optimal semantic representation with two transformer decoder layers, as too few layers under-express feature relations and too many risk rank collapse [18]. Lastly, FL2T maintains superior scores across all LoRA ranks (Table 4), outperforming CIDM (rank = 4) even at a lower rank with 25% fewer parameters, highlighting the parameter efficiency of our approach.

Number of reference images	Methods	V1 - V5		V6 - V10		Avg.	
		IA (\uparrow)	TA (\uparrow)	IA (\uparrow)	TA (\uparrow)	IA (\uparrow)	TA (\uparrow)
1	CIDM	76.6	<u>79.5</u>	69.7	<u>74.5</u>	73.2	<u>77.0</u>
	Ours	80.0	78.7	72.5	74.1	76.3	76.4
2	CIDM	78.1	<u>79.2</u>	71.2	<u>74.2</u>	74.6	<u>76.7</u>
	Ours	80.4	78.7	72.1	74.0	76.3	76.3
3	CIDM	80.8	<u>78.2</u>	72.1	73.6	76.4	75.9
	Ours	82.3	<u>79.0</u>	73.7	<u>73.9</u>	78.0	<u>76.4</u>
≥ 4	CIDM	84.0	<u>77.3</u>	71.7	72.6	78.0	74.8
	Ours	84.9	77.0	74.8	<u>88.9</u>	79.8	<u>75.4</u>

Number of reference	Methods	IMS (\uparrow)	FID (\downarrow)	IMS (\uparrow)	FID (\downarrow)	IMS (\uparrow)	FID (\downarrow)
		1	CIDM	61.7	199.0	55.3	<u>291.8</u>
	Ours	65.0	<u>179.2</u>	54.7	292.4	59.9	<u>235.8</u>
2	CIDM	66.5	178.3	57.8	284.9	62.2	231.6
	Ours	69.0	<u>165.5</u>	58.1	<u>278.8</u>	63.6	<u>222.1</u>
3	CIDM	71.3	156.5	58.5	285.3	64.9	220.9
	Ours	72.0	<u>152.9</u>	60.3	<u>272.7</u>	66.2	<u>212.8</u>
≥ 4	CIDM	74.0	142.0	61.5	270.0	67.7	206.0
	Ours	78.2	<u>133.3</u>	64.4	<u>262.7</u>	71.3	<u>198.0</u>

Table 3. Comparison of model performances with different number of reference images. IA and TA refer to CLIP [32] Image Alignment and Text Alignment scores respectively. The best IA and IMS scores have been denoted in **bold**, and the TA and FID values have been underlined.

A.2. Datasets, Implementation Details and Evaluation Metrics

Datasets. We evaluate our approach on three datasets, each selected to ensure strong semantic alignment with our task objectives (Fig. 6). For the CIFC dataset [5], we adopt the benchmark established in the original paper, which features visually rich concept cards designed to challenge models in hallucination detection. For the ImageNet [4] subset, we manually select 3–5 images per class from ten classes, ensuring that each image contains a well-centered, unobstructed primary object. For the CelebA dataset [26], we construct a subset of ten identities, with 3–5 representa-

LoRA rank	Methods	V1 - V5		V6 - V10		Avg.	
		IA (\uparrow)	TA (\uparrow)	IA (\uparrow)	TA (\uparrow)	IA (\uparrow)	TA (\uparrow)
3	CIDM	82.3	<u>78.3</u>	71.9	72.4	77.1	75.3
	Ours	84.5	77.6	73.8	<u>88.6</u>	79.1	<u>75.6</u>
4	CIDM	84.0	<u>77.3</u>	71.7	72.6	78.0	74.8
	Ours	84.9	77.0	74.8	<u>88.9</u>	79.8	<u>75.4</u>
5	CIDM	82.5	<u>78.1</u>	73.1	72.9	77.8	75.4
	Ours	85.4	77.3	74.7	<u>73.7</u>	80.1	<u>75.5</u>
6	CIDM	82.7	<u>78.3</u>	73.0	73.0	77.9	75.6
	Ours	84.4	77.7	73.1	<u>74.2</u>	78.7	<u>76.0</u>

LoRA rank	Methods	IMS (\uparrow)	FID (\downarrow)	IMS (\uparrow)	FID (\downarrow)	IMS (\uparrow)	FID (\downarrow)
		3	CIDM	72.6	150.3	62.2	<u>262.7</u>
	Ours	76.6	<u>135.1</u>	61.8	263.9	69.2	<u>199.5</u>
4	CIDM	74.0	142.0	61.5	270.0	67.7	206.0
	Ours	78.2	<u>133.3</u>	64.4	<u>262.7</u>	71.3	<u>198.0</u>
5	CIDM	73.5	145.4	62.4	<u>260.2</u>	68.0	202.8
	Ours	76.8	<u>132.5</u>	63.3	263.7	70.1	<u>198.1</u>
6	CIDM	72.6	147.1	61.7	<u>267.2</u>	67.1	207.2
	Ours	76.7	<u>134.8</u>	60.9	273.3	68.9	<u>204.0</u>

Table 4. Comparison of model performances for different LoRA [15,45] configurations. IA and TA refer to CLIP [32] Image Alignment and Text Alignment scores, respectively. The better IA and IMS scores have been denoted in **bold**, and TA and FID values have been underlined.

tive images per identity. Images are chosen based on clear frontal facial orientation, uniform lighting, and minimal occlusion to preserve identity consistency. This hand-curated dataset design provides high-quality supervision, which is crucial for minimizing semantic hallucinations and promoting accurate visual-textual alignment.

For the experiments on varying numbers of reference images (Table 3), we have used a fixed set of images picked randomly (without human intervention).

Implementation Details. We use Stable Diffusion (SD-1.5) [35] as the pretrained model for all experiments. The training is conducted with a fixed initial learning rate of 1.0×10^{-3} for updating textual embeddings and 1.0×10^{-4} for optimizing the U-Net. Empirically, we set $\gamma_1 = 0.1$ and $\gamma_2 = 0.1$ in Eq. 6.

Evaluation Metrics. Following the experiments under our problem setting as in Sec 3, we evaluate our generated images across 2 metrics - Image Alignment (IA) and Text Alignment (TA). Image Alignment (IA) scores are computed using CLIP [32] image encoder, comparing the similarity of features between generated images and reference images. Similarly, we utilize the text encoder of CLIP [32] to evaluate the text-image similarity between the input prompt and synthesized image for the Text Alignment (TA) scores. Additionally, we utilize *Identity Matching Score (IMS)* that measures the semantic closeness of the generated image and reference image [25]. It is computed as the cosine similarity score between embeddings of generated images and mean of reference image embeddings. For the CIFC dataset [5] and the ImageNet dataset [4], we utilize ResNet-152 [13] as the image encoder. On the other hand,

Methods	V1		V2		V3		V4		V5		V6		V7		V8		V9		V10		Avg.		
	IMS (↑)	FID (↓)	IMS (↑)	FID (↓)	IMS (↑)	FID (↓)	IMS (↑)	FID (↓)	IMS (↑)	FID (↓)	IMS (↑)	FID (↓)	IMS (↑)	FID (↓)	IMS (↑)	FID (↓)	IMS (↑)	FID (↓)	IMS (↑)	FID (↓)	IMS (↑)	FID (↓)	
CIFU [5]	CIDM [5]	84.7	82.2	74.5	166.1	66.7	156.7	65.1	211.9	78.9	93.2	53.6	348.4	80.8	119.0	49.7	345.6	70.0	195.6	53.3	341.5	67.7	206.0
	Ours with proxy-guidance	87.7	71.8	75.1	169.3	75.6	145.4	71.3	202.5	81.1	77.7	55.8	355.2	89.5	98.4	48.3	353.4	69.8	189.9	58.6	316.4	71.3	198.0
	Δ	+3.0	-10.4	+0.6	+3.2	+8.9	-11.3	+6.2	-8.6	+2.2	-15.5	+2.2	+6.8	+8.7	-20.6	-1.4	+7.8	-0.2	-5.7	+5.3	-25.1	+3.6	-8.0
CelebA [26]	CIDM [5]	63.9	233.2	65.6	219.7	60.1	250.0	76.0	166.8	55.3	246.7	61.4	234.5	58.0	193.4	56.1	273.5	51.2	185.7	57.0	197.0	60.5	220.0
	Ours with proxy-guidance	64.4	225.8	69.3	212.2	63.5	239.8	70.2	168.9	57.4	188.7	63.9	221.1	58.1	218.0	59.5	236.9	55.4	170.4	63.0	195.4	62.5	209.0
	Δ	+0.5	-7.4	+3.7	-7.5	+3.4	-10.2	-5.8	+2.1	+2.1	-58.0	+2.5	-13.4	+0.1	+24.6	+3.4	-36.6	+4.2	-15.3	+6.0	-1.6	+2.0	-11.0
Inet [5]	CIDM [5]	81.6	129.6	68.3	113.6	85.4	75.7	85.0	85.1	73.5	91.5	78.4	86.2	64.9	135.1	79.4	58.8	80.1	88.1	87.4	57.3	78.4	92.1
	Ours with proxy-guidance	85.2	103.1	75.2	107.1	88.5	57.1	84.1	79.3	85.7	83.5	84.8	69.1	75.6	110.3	77.2	64.3	80.2	79.8	95.4	31.6	83.2	78.5
	Δ	+3.6	-26.5	+7.1	-6.5	+3.1	-18.6	-0.9	-6.2	+12.2	-8.0	+6.4	-17.1	+10.7	-24.8	-2.2	+5.5	+0.1	-8.3	+8.0	-25.7	+4.8	-13.6

Table 5. **Additional Experiments.** FL2T outperforms CIDM across the three datasets on Identity Matching Scores (IMS) [25] and Fretchet Inception Distance (FID) [17], effectively showcasing its ability to preserve identities better and improved generation capabilities.

we have utilized VGG-Face [38] for CelebA [26]. Further, *Fretchet Inception Distance (FID)* evaluates the quality and diversity of images by comparing the Inception-v3 feature distributions of the reference images and generated images [17].

A.3. Additional Experiments

Beyond CLIP scores, we utilize two other metrics, *Identity Matching Score (IMS)* and *Fretchet Inception Distance (FID)*. IMS that measures the semantic closeness of the generated image and reference image [25]. Specifically, this metric is designed to measure the identity match between of the concepts in generated images. Whereas FID compares the distributions of generated and reference images using Inception-v3 features [17]. Based on these metrics, as shown in Table 5, we observe that FL2T outperforms CIDM across the three datasets, showing trends akin to CLIP [32] scores.

On comparison with Multi-concept Customization [20], FL2T delivers consistent identity gains, boosting IMS by 12–31 points across concepts, with strong IA improvements on most concepts. Importantly, it achieves lower (better) FID indicating high quality image generation results as shown in Table 6.

A.4. Comparing Attention and Concatenation Operations

The main contribution of this work revolves around “positively” exploiting the higher-order interactions between concepts. Towards this end, we analyze two operations that are commonly utilized to extract richer representations from a set of embeddings. Consider a set of embeddings, $S = \{X, Y, Z\} \in \mathbb{R}^d$. We assume that trivial components such as linear layers for scaling in attention and downsampling in concatenation are present.

Attention. Attention computes the cosine similarity between X and Y and adds the projected component of X on Y to X -

$$\text{Attn}(X; (X, Y)) = X + (X \cdot Y^T)Y$$

To develop a deeper understanding, we consider three vectors and let a_{XY} be the cosine similarity between vectors X and Y . Then, after the first attention operation where $S_1 = \{X_1, Y_1, Z_1\}$ is the output :

$$\begin{aligned} X_1 &= X + a_{XY}Y + a_{XZ}Z \\ Y_1 &= a_{XY}X + Y + a_{YZ}Z \\ Z_1 &= a_{XZ}X + a_{YZ}Y + Z \end{aligned}$$

Subsequently, extending this to a second attention layer provides us:

$$\begin{aligned} x_2 &= [1 + (a_{XY}^2 + a_{XZ}^2)(a_{XY}^2 + a_{YZ}^2 + a_{XZ}^2 + 3) + 6a_{XY}a_{YZ}a_{XZ}]X \\ &\quad + [a_{XY}(3a_{YZ}^2 - 2) + (a_{XY} + a_{XZ}a_{YZ})(a_{XY}^2 + a_{YZ}^2 + a_{XZ}^2 + 6)]Y \\ &\quad + [a_{XZ}(3a_{YZ}^2 - 2) + (a_{XZ} + a_{XY}a_{YZ})(a_{XY}^2 + a_{YZ}^2 + a_{XZ}^2 + 6)]Z \end{aligned}$$

The number of pairwise interactions between the vectors of S has significantly increased in the second attention layer, thereby allowing the model to capture higher-level dependencies between the vectors. It is important to note that attention is a generalized form of weighted aggregation.

Concatenation. On the other hand, concatenation captures non-linear interactions between each element of the vectors. This can introduce unintended noise and alter the original embedding negatively. The operation is defined below where a_i , b_i and c_i are polynomials for the i -th element.

$$\text{Concat}(X, Y, Z) = \sum_{i=0}^{d-1} a_i X_i + b_i Y_i + c_i Z_i$$

A.5. Bounding Model Drift under Unnormalized Attention Coefficients

We quantify one-step model drift by the norm of the aggregated gradient. Lemma A.1 shows a universal upper bound (the same crude bound as uniform summation), and Theorem A.1 gives a simple, explicit construction proving that unnormalized attention can *strictly reduce* drift relative to uniform summation.

Methods	V1		V2		V3		V4		V5		V6		V7		V8		V9		V10		Avg.	
	IA (↑)	TA (↑)	IA (↑)	TA (↑)	IA (↑)	TA (↑)	IA (↑)	TA (↑)	IA (↑)	TA (↑)	IA (↑)	TA (↑)	IA (↑)	TA (↑)	IA (↑)	TA (↑)	IA (↑)	TA (↑)	IA (↑)	TA (↑)	IA (↑)	TA (↑)
Multi-concept Customization [20]	74.4	77.6	76.6	73.4	73.4	74.7	69.7	73.9	78.2	80.7	65.9	76.0	73.6	66.3	68.7	76.2	62.7	75.8	71.2	83.5	71.4	75.8
Ours with proxy guidance	84.4	74.0	86.1	81.6	84.4	70.1	82.2	81.1	87.2	78.0	69.3	72.9	85.3	70.4	60.7	77.6	82.1	76.6	76.5	71.6	79.8	75.4
Δ	+10.0	-3.6	+9.5	+8.2	+11.0	-4.6	+12.5	+7.2	+9.0	-2.7	+3.4	-3.1	+11.7	+4.1	-8.0	+1.4	+19.4	+0.8	+5.3	-11.9	+8.4	-0.4
Methods	IMS (↑)	FID (↓)	IMS (↑)	FID (↓)	IMS (↑)	FID (↓)	IMS (↑)	FID (↓)	IMS (↑)	FID (↓)	IMS (↑)	FID (↓)	IMS (↑)	FID (↓)	IMS (↑)	FID (↓)	IMS (↑)	FID (↓)	IMS (↑)	FID (↓)	IMS (↑)	FID (↓)
Multi-concept Customization [20]	65.4	160.9	62.8	98.7	64.1	189.5	63.7	222.6	66.2	86.5	67.8	386.6	61.9	91.2	60.5	386.9	62.3	220.0	64.8	379.3	63.5	216.2
Ours with proxy guidance	85.2	71.8	75.2	169.3	88.5	145.4	84.1	202.5	85.7	77.7	84.8	355.2	75.6	98.4	77.2	353.4	80.2	189.9	95.4	316.4	83.2	198.0
Δ	+19.8	-7.3	+12.4	-8.4	+24.4	+44.1	+20.4	+20.1	+19.5	+8.8	+17.0	+31.4	+13.7	-7.2	+16.7	+33.5	+17.9	+20.1	+30.6	+62.9	+19.7	+18.2

Table 6. **Comparison with multi-concept method.** We compare FL2T with Multi-concept customization [20] on the CIFC dataset [5] across all metrics, CLIP Image Alignment (IA), CLIP Text Alignment (TA), Identity Matching Scores (IMS) [25] and Fretchet Inception Distance (FID) [17], and notice that FL2T outperforms Multi-concept Customization across all metrics.

Operation	Pairwise Interactions (per layer)	After M Layers	Permutation Invariance
Summation ($x + y$)	nd	Mnd	✓
Concatenation ($[x; y]$)	0	0	✓
Attention	n^2d	Mn^2d	✓

Table 7. **Pairwise interactions.** We compute the number of pairwise interactions for combining two vectors $x, y \in \mathbb{R}^d$ across n embeddings. We assume the same k, d for M layers. The attention function showcases its superiority by showing the largest number pairwise interactions and is permutation invariant.

Setup and Assumptions Let $(\mathbb{R}^d, \langle \cdot, \cdot \rangle)$ be a real inner-product space with norm $\|v\| = \sqrt{\langle v, v \rangle}$. We have N concepts with losses $\ell_i(\theta)$ and gradients

$$m_i := \nabla_{\theta} \ell_i(\theta) \in \mathbb{R}^d, \quad i = 1, \dots, N.$$

We compare two aggregate gradients:

$$M_{\text{CIDM}} := \sum_{i=1}^N m_i$$

$$M_{\text{FL2T}} := \sum_{i=1}^N \lambda_i m_i, \quad \lambda_i \in [-1, 1].$$

We impose *no* normalization on (λ_i) (in particular, $\sum_i \lambda_i$ need not equal 1). One-step drift with learning rate $\eta > 0$ is proportional to $\|M\|$, so we compare $\|M_{\text{FL2T}}\|$ to $\|M_{\text{CIDM}}\|$.

Lemma A.1 (Universal Upper Bound). *For any coefficients $\lambda_i \in [-1, 1]$,*

$$\|M_{\text{FL2T}}\| = \left\| \sum_{i=1}^N \lambda_i m_i \right\| \leq \sum_{i=1}^N |\lambda_i| \|m_i\| \leq \sum_{i=1}^N \|m_i\|.$$

Proof. By the triangle inequality and homogeneity of norms,

$$\left\| \sum_{i=1}^N \lambda_i m_i \right\| \leq \sum_{i=1}^N \|\lambda_i m_i\| = \sum_{i=1}^N |\lambda_i| \|m_i\| \leq \sum_{i=1}^N \|m_i\|$$

because $|\lambda_i| \leq 1$ for all i . \square

Theorem A.1 (Existence of Reduced Drift). *If $M_{\text{CIDM}} \neq 0$, then there exists $\lambda \in [-1, 1]^N$, not all equal to 1, such that $\|M_{\text{FL2T}}\| < \|M_{\text{CIDM}}\|$.*

Proof. Set $M_{\text{CIDM}} = \sum_{k=1}^N m_k$. Then

$$\begin{aligned} \sum_{k=1}^N \langle M_{\text{CIDM}}, m_k \rangle &= \left\langle M_{\text{CIDM}}, \sum_{k=1}^N m_k \right\rangle \\ &= \langle M_{\text{CIDM}}, M_{\text{CIDM}} \rangle \\ &= \|M_{\text{CIDM}}\|^2 > 0. \end{aligned}$$

Consequently, there exists an index k^* for which

$$\langle M_{\text{CIDM}}, m_{k^*} \rangle > 0.$$

Fix such an index k^* . For any $\varepsilon \in (0, 1]$, define coefficients

$$\lambda_{k^*} = 1 - \varepsilon, \quad \lambda_j = 1 \quad \text{for all } j \neq k^*.$$

These coefficients lie in $[-1, 1]$ and are not all equal to 1, so the resulting vector

$$M_{\text{FL2T}} = \sum_{i=1}^N \lambda_i m_i = M_{\text{CIDM}} - \varepsilon m_{k^*}$$

is feasible. Expanding the squared norm yields

$$\begin{aligned} \|M_{\text{FL2T}}\|^2 &= \|M_{\text{CIDM}} - \varepsilon m_{k^*}\|^2 \\ &= \|M_{\text{CIDM}}\|^2 - 2\varepsilon \langle M_{\text{CIDM}}, m_{k^*} \rangle + \varepsilon^2 \|m_{k^*}\|^2 \end{aligned}$$

Since $\langle M_{\text{CIDM}}, m_{k^*} \rangle > 0$, the quadratic expression on the right-hand side is strictly smaller than $\|M_{\text{CIDM}}\|^2$ whenever

$$0 < \varepsilon < \min \left\{ 1, \frac{2 \langle M_{\text{CIDM}}, m_{k^*} \rangle}{\|m_{k^*}\|^2} \right\}.$$

Thus $\|M_{\text{FL2T}}\|^2 < \|M_{\text{CIDM}}\|^2$, which implies $\|M_{\text{FL2T}}\| < \|M_{\text{CIDM}}\|$. Hence, there exists a feasible coefficient vector λ strictly reducing the norm, completing the proof. \square

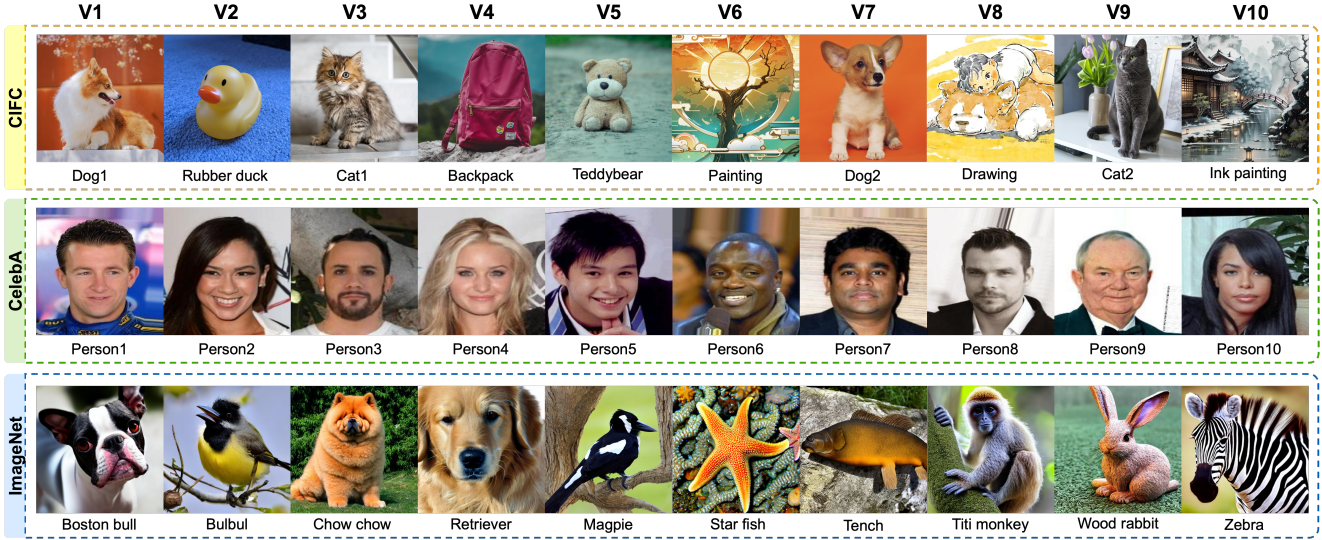


Figure 6. **Datasets used for the experiments.** We present an overview of the images used in our experiments for the CIDM [5], CelebA [26] and ImageNet [4] datasets.

Remark (degenerate case). If $M_{\text{CIDM}} = 0$, then $\|M_{\text{CIDM}}\| = 0$ is already minimal, so no strict decrease is possible; nonetheless, Lemma A.1 still holds.

A.6. Background on Custom Diffusion Models.

Latent diffusion models (LDMs) [8, 37] rely on conditional inputs, such as text prompts [31, 34] or images [16, 30], to guide the generation of images. These models utilize an encoder $E(\cdot)$ and a decoder $D(\cdot)$ to facilitate image synthesis in the latent space. Custom diffusion models (CDMs) [7, 11, 27] extend LDMs by incorporating low-rank adaptation (LoRA) [15, 45] to fine-tune pretrained diffusion models [1, 35] for personalized concept learning.

Given a personalized image-text pair (x, p) , the encoder $E(\cdot)$ maps x to a latent representation z , with z_t denoting the noisy latent feature at timestep t ($t = 1, \dots, T$). The text encoder $\Gamma(\cdot)$, such as a pretrained CLIP model [32], maps the text prompt p to a textual embedding $c = \Gamma(p)$. The objective for learning a personalized concept (x, p) at timestep t is defined as:

$$L_{\text{CDM}} = \mathcal{E}_{z \sim E(x), c, \varepsilon \sim \mathcal{N}(0, I), t} [\|\varepsilon - \varepsilon_{\theta'}(z_t | c, t)\|_2^2] \quad (7)$$

where $\varepsilon_{\theta'}(\cdot)$ represents the denoising UNet [31, 35] that gradually denoises z_t by estimating the Gaussian noise $\varepsilon \sim \mathcal{N}(0, I)$. The parameter set θ' corresponds to $\theta' = \theta_0 + \Delta\theta$, where $\theta_0 = \{W_l^0\}_{l=1}^L$ denotes the pretrained weights in LDMs, and $\Delta\theta = \{\Delta W_l\}_{l=1}^L$ corresponds to the LoRA-updated parameters [9, 20]. Here, $W_l^0, \Delta W_l \in \mathbb{R}^{a \times b}$ are the pretrained and low-rank weight matrices in the l -th transformer layer of θ' , respectively, where a and b are matrix

dimensions. Following [36, 53], the low-rank update ΔW_l can be factorized as $\Delta W_l = A_l B_l$, where $A_l \in \mathbb{R}^{a \times r}$ and $B_l \in \mathbb{R}^{r \times b}$ with rank $r \ll \min(a, b)$.

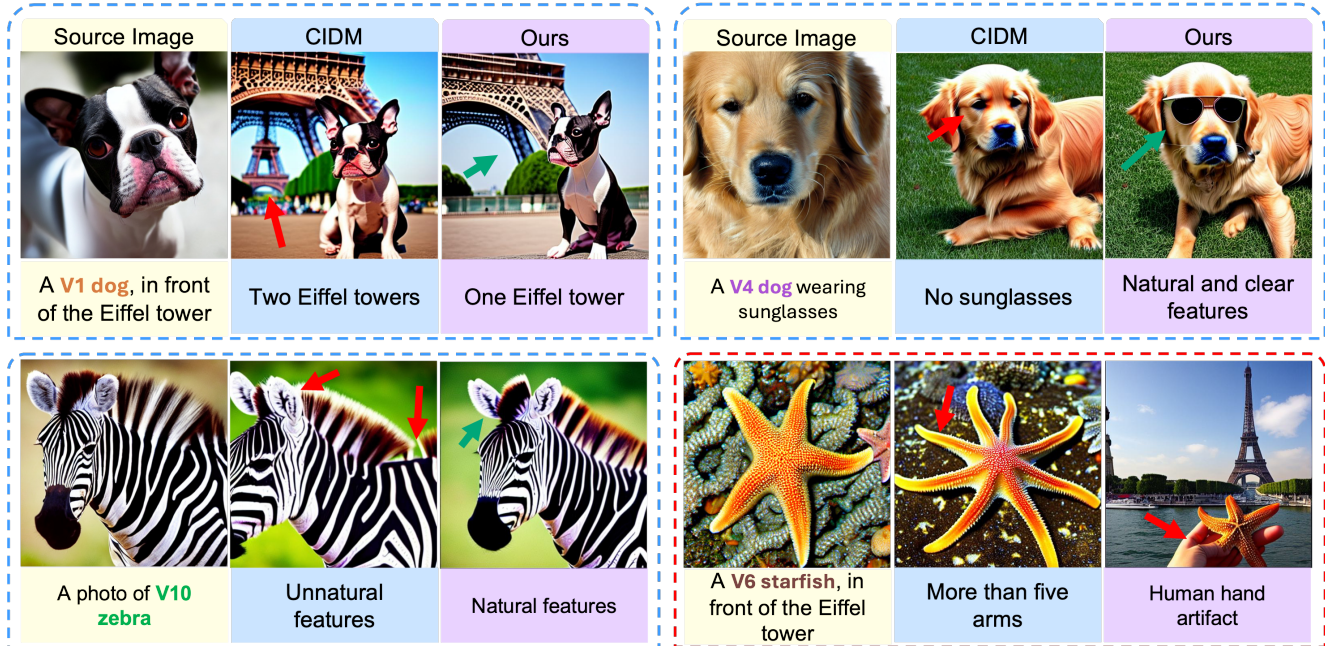


Figure 7. **Qualitative Analysis on the ImageNet dataset [4].** We compare the synthesized images by CIDM [5] and FL2T (Ours). The images are generated with a source image and an associated text prompt as input. Images with red and green arrows indicate regions of undesirable and desirable qualities, and their reasons are stated below each image. FL2T preserves features and conforms to the text prompt better than CIDM. We have also shown a failure case of FL2T (bottom right in red box), where we observe a human hand artifact, but the identity of the starfish is preserved (only five arms).

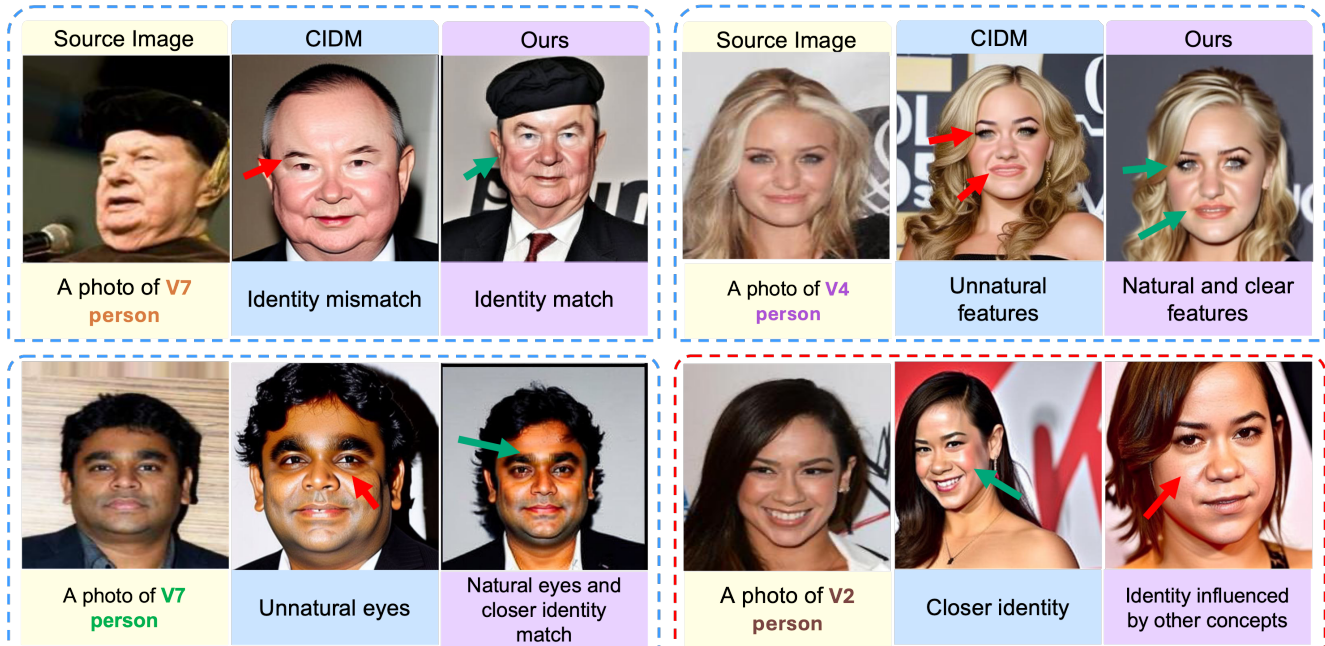


Figure 8. **Qualitative Analysis on the CelebA dataset [26].** We compare the synthesized images by CIDM [5] and FL2T (Ours). The images are generated with a source image and an associated text prompt as input. Images with red and green arrows indicate regions of undesirable and desirable qualities, and their reasons are stated below each image. FL2T preserves identity and features better than CIDM. We have also shown a failure case of FL2T (bottom right in red box), where the identity of V2 person was influenced by other concepts in the dataset.

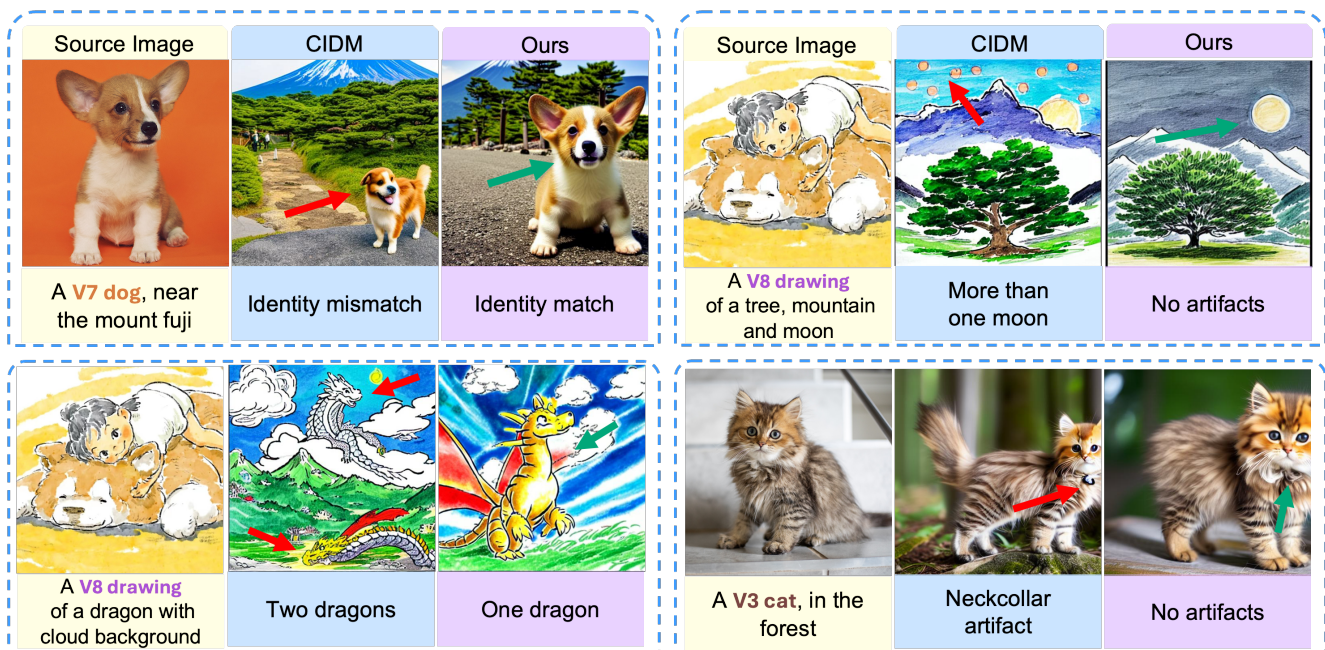


Figure 9. **More Qualitative Samples on the CIFC dataset [5].** We compare the synthesized images by CIDM [5] and FL2T (Ours). The images are generated with a source image and an associated text prompt as input. Images with red and green arrows indicate regions of undesirable and desirable qualities, and their reasons are stated below each image.